MATERIALS PHYSICS AND MECHANICS RESEARCH ARTICLE

Submitted: August 18, 2025 **Revised: October 24, 2025** **Accepted: November 29, 2025**

Experimental and numerical study of energy absorption in bio-inspired scutoid cellular structures

Y. Sepahvand, F. Morshedsolouk ✉, A. Moazemi Goudarzi

Babol Noshirvani University of Technology, Babol, Mazandaran, Iran

✉ f.morshed@nit.ac.ir

ABSTRACT

This study investigates the compressive behavior and energy absorption of bio-inspired scutoid cellular structures made from polylactic acid to enhance mechanical energy absorbers used in impact protection. Seven four-cell scutoid specimens with varied transition point positions and wall thicknesses were fabricated using additive manufacturing and tested under quasi-static compression. Numerical simulations were conducted using finite element analysis in Abaqus to complement the experiments. Results show that scutoid structures outperform equivalent honeycomb designs in energy absorption efficiency, with the highest performance achieved when the transition point is located near the mid-height of the cells. Increasing wall thickness improves all key energy absorption indicators. Design of experiments reveals inner wall thickness as the most significant factor affecting energy absorption. The findings demonstrate that optimizing transition point location and wall thickness significantly enhances the crashworthiness of scutoid structures, making them promising candidates for lightweight energy absorbers.

KEYWORDS

PLA 3D-printed scutoid • energy absorption • crushing • explicit dynamics • crushing test

Citation: Sepahvand Y, Morshedsolouk F, Moazemi Goudarzi A. Experimental and numerical study of energy absorption in bio-inspired scutoid cellular structures. *Materials Physics and Mechanics*. 2025;53(6): 63–81. http://dx.doi.org/10.18149/MPM.5362025_6

Introduction

Mechanical energy absorbers are structures that convert all or part of the impact kinetic energy into potential strain energy. Since 1952, when a patent about a crumple zone was issued, mechanical energy absorbers have been used in various industries, such as automotive, railway, shipbuilding, and military industries [1]. Crumple zones, also known as crash boxes, are lightweight tubes that absorb collision energy and minimize the effect of collision impact on passengers, thereby increasing passengers' safety [2]. These energy-absorbing structures are usually subjected to axial compressive load, and the quasi-static compression test is a simple method to evaluate structures' energy absorption capability. Increasing the efficiency of energy absorbers is possible by either increasing the amount of absorbed energy (EA) or reducing the peak crushing force (PCF) in the quasi-static compression test. Researchers have been trying to enhance energy absorbers' efficiency by comprehending the behavior of conventional structures or introducing contemporary designs.

The first serious discussions and analyses of the compressive behavior of thin-walled circular tubes under quasi-static loads emerged during the 1960s with Alexander [3], who studied cylindrical tubes as a passive energy absorbing method and developed an empirical formula to predict the PCF for thin-walled cylinders. Abramovich

and Jones [4,5] performed a series of static and dynamic collapse tests on cylindrical and square tubes, modified Alexander's formula for the axisymmetric buckling failure mode of the cylinders and suggested the PCF empirical formula for the square tubes. Tak and Iqbal [6] compared the performance of square and circular tubes under impact load.

A great deal of previous research into energy-absorbing structures has mainly focused on enhancing tubes' energy absorption capacity by filling them with foam. For instance, Yamada et al. [7], Zarei et al. [8], and Zhibin et al. [9] investigated the absorbed energy and the collapse behavior of foam-filled aluminum tubes. Another method is using functionally graded foams and foams with different densities to improve the tube's energy absorption capacity [10]. However, filling tubes with lattice and cellular structures can improve the energy absorption performance of the tubes, as well. This idea was studied by Baykasoğlu et al. [11], Cetin and Baykasoğlu [12], and Tao et al. [13]. Moreover, Le et al. [14] and Nikkhah et al. [15] suggested a new stepwise lattice-filled structure to maintain a high compressive load after first buckling and improve the efficiency of the energy absorption. Hosseinpour et al. [16] conducted both numerical and experimental analyses on thin-walled auxetic cylindrical tubes (featuring Cylindrical Lozenge Grid, Square Grid, and Peanut Grid patterns) under quasi-static axial compression. Their findings emphasized that pattern type and rib thickness (porosity) significantly influence energy dissipation and failure modes, concluding that careful design can prioritize controlled and predictable deformation.

Other researchers suggested that the lower the PCF is, the higher the energy absorption efficiency is. They concluded that introducing imperfections, such as dents, grooves, or corrugation, may decrease the first buckling force, and consequently, the energy absorption process will be more efficient. Nikkhah et. al. [17], and Rogala et al. [18] reduced PCF by creating grooves on the circular, square. Whereas Tran et. al. [19], Taghipour et al. [20], and El-Baky et al. [21] argued that although holes can decrease PCF, they may cause major implications on energy absorption and can decrease the energy absorption capacity.

Following the introduction of the additive manufacturing method, many researchers use 3D-printed complicated structures for energy absorption applications, i.e., 3D-printed FGM structures are common shapes. Borovkov et al. [22] studied the mechanical properties of 3D printed meta materials. Baroutaji et al. [23] investigated a metal FGT 3D-printed circular section under transverse loading. By changing the FGT pattern they succeeded in improving the energy absorption capacity by 79%. Nian et al. [24,25] studied the energy absorption of the tube filled with FGM lattice and used an optimization method to increase the energy absorption. Similarly, Gharehbaghi and Farrokhabadi [26] utilized additive manufacturing to evaluate the energy absorption capability of a novel cruciform composite lattice structure made from continuous glass fiber reinforced polymer, highlighting the need for innovative printing paths to prevent debonding in complex cell joints. Focusing on enhanced structural topology, Gharehbaghi et al. [27] and Ghorbani et al. [28] introduced a new lattice structure for energy absorption applications. Ghorbani et al. [29] investigated a bone-inspired composite cellular structure fabricated using fused deposition modeling (FDM) 3D printing from glass fiber-reinforced polylactic acid (PLA).

Moreover, to date, several studies have begun to examine the use of bio-inspired cellular structures as energy absorbers. Among them, honeycomb is a well-known geometry that has been used for many structural applications. The structure of the basic form of the honeycomb is studied by Galehdari et al. [30] and Gu et al. [31]. While, Usta et al. [32], Feng et al. [33], Xia et al. [34], Nikhah et al. [35], and Tau et al. [36] studied the crushing behavior of the honeycombs with more complex geometries, i.e., graded honeycomb and hierarchical honeycomb.

A scutoid is a complex three-dimensional bio-inspired cellular structure that can be found in the epithelial tissues of organisms and is highly efficient in stabilizing packing structures [37]. Dehiri and Patel [38], for the first time, studied the compressive behavior of the aluminum scutoids self-packing cell numerically using ABAQUS software. To the authors' best knowledge, no experimental studies have been paired with numerical analyses. To fill the gap, this paper presents an experimental and numerical investigation of the compressive behavior and energy absorption characteristics of polymetric scutoid-based cellular structures under quasi-static compressive loading. For this purpose, sets of self-packing scutoids consisting of four cells are designed and fabricated through additive manufacturing using PLA filament and are tested under a quasi-static compression load. The energy absorption performance of these cellular structures is also studied numerically in the explicit dynamic module of Abaqus software.

Materials and Methods

A scutoid is composed of two parallel polygon or polygon-like shapes whose vertexes are connected through lines, curves, and at least a Y-shaped edge. The scutoid structures are widely observed in the living creatures' hard curved shells which have high compressive strength. The scutoid's transition point is the bifurcation point on the Y-shape edge (Fig. 1). Scutoids are efficient shapes in packing cellular shapes between two parallel surfaces.

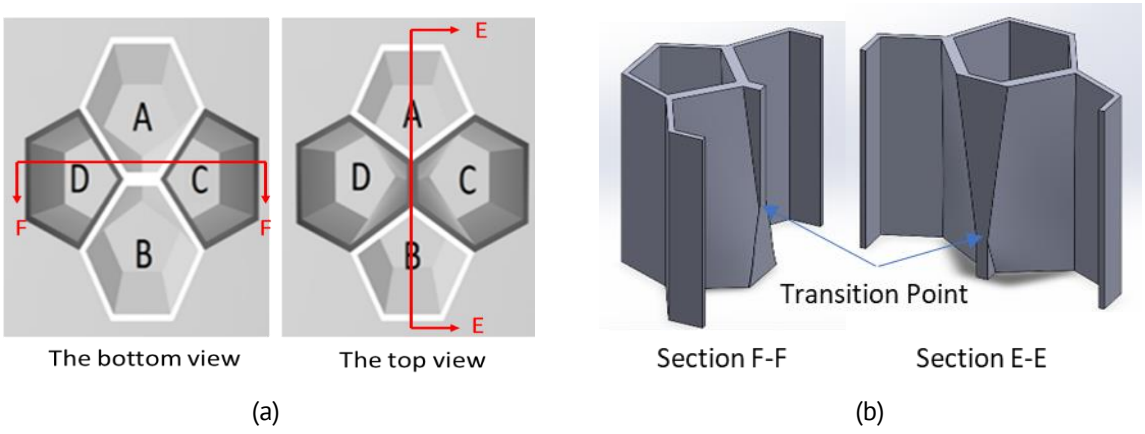

Fig. 1. The top and bottom view (a) and details of the self-packing four-cells scutoid (b)

In this research, the compressive behavior of a four-cell structure consisting of polymeric scutoids elements is investigated experimentally and numerically and the effect of the location of the transition point on the energy absorption and the crushing behavior is studied. Moreover, an equivalent honeycomb structure is used as a comparison basis. Seven cellular structures consisting of four self-packing scutoids are

modeled and their compressive behavior is analyzed in Abaqus software. These structures are also made through additive manufacturing and tested under a compressive load.

Scutoid structure design

The studied scutoid geometry is shown in Figs. 1 and 2. It is composed of two pentagons and two hexagons on the top and bottom planes. A hexagon on the top plane (or on the bottom plane) is connected to a polygon on the bottom plane (or on the top plane) by 4 lines and a Y-shaped edge (Fig. 1(a)). The transition point is defined as the bifurcation point of the Y-shape edge and is shown in Fig. 1(b) in the section views. The cells have two hexagonal and two pentagonal cross-sections in the top and bottom planes with an edge length of 6 mm. According to these dimensions, all specimens have the same relative density. As mentioned before, an equivalent honeycomb structure is also studied as a comparison basis.

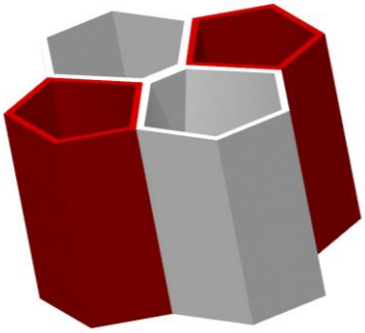

Fig. 2. The self-packing four-cells scutoid

All specimens have a fixed length of 20 mm, so for T20, the transition point is positioned 4 mm from the base. The scutoid specimens used in this study are divided into two distinct groups based on wall thickness configurations:

1. Group A: These models correspond to the specimens described in the Methodology section, where the inner walls have a thickness of 1 mm, which is twice the thickness of the outer walls at 0.5 mm.
2. Group B: This separate set of models was specifically designed to analyze the effect of wall thickness by using uniform wall thicknesses for both inner and outer walls.

For both groups, the specimens are labeled with the letter "T" followed by a number (e.g., T20, T30, ..., T80), which indicates the percentage height of the transition point relative to the total height of the scutoid. For example, T20 refers to a specimen whose transition point is located at 20% (0.2) of the total height from the base (lower) plane. The specimens in Group B are labeled with the transition point percentage followed by the wall thickness, for example, "T50 0.5 mm" indicates a specimen with a transition point at 50 % height and uniform wall thickness of 0.5 mm.

Additive manufacturing of specimens

Additive manufacturing can be used to create complex geometries. In this research, the four-cell scutoid specimens are fabricated using Dayan K36P 3D printer (Fig. 3). The 3D

models of the specimens were first designed in SOLIWORKS software and imported into ULTIMAKER CURA software in STL format. Then, the printer setup is implemented and the G-CODE files are developed to print the samples. The 3D printer settings for the specimens' fabrication are shown in Table 1.

Table 1. 3D printing process characterization

Filament material	PLA
Nozzle diameter, mm	0.5
Nozzle temperature, °C	200
Bed surface temperature, ˚C	50
Layer height, mm	0.2
Internal density, %	100

Fig. 3. The scutoid and honeycomb specimens fabricated by 3D printer

PLA material properties

The specimens are made of PLA using additive manufacturing. The PLA material properties are given in Table 2. In the finite element model, the mechanical behavior before the yield point is described by the elastic modulus, Poisson's ratio, and density. In the post-yield stage, the piecewise linear elastic-plastic model is defined by the experimental stress-strain curve of the standard specimen. Since no obvious fracture can be detected in the specimens during quasi-static experiments, the fracture and damage are not considered in the numerical simulations.

Table 2. The basic material parameters of PLA [33]

Density, kg/m^3	**Elastic modulus, GPa**	**Poisson's ratio**	**Yield strength, MPa**	**Initial yield strain**
1200	1.97	0.35	40	0.026

Experimental procedure

Energy absorption and crushing behavior of seven scutoid specimens and a honeycomb specimen were investigated under quasi-static compressive load. The specimens were made of PLA filament using an additive manufacturing process and were tested using SANTAM STM20 compression test device. As shown in Fig. 4 each specimen was placed between test machine platens, then, the upper platen moved downward with constant speed, while the lower platen was fixed. To fulfill the quasi-static criterion, the compression rate of 2 mm/min is applied. A load cell measured the crushing force at each displacement interval and the force–displacement diagrams are extracted, so that the behavior of the specimens during the test can be evaluated and compared.

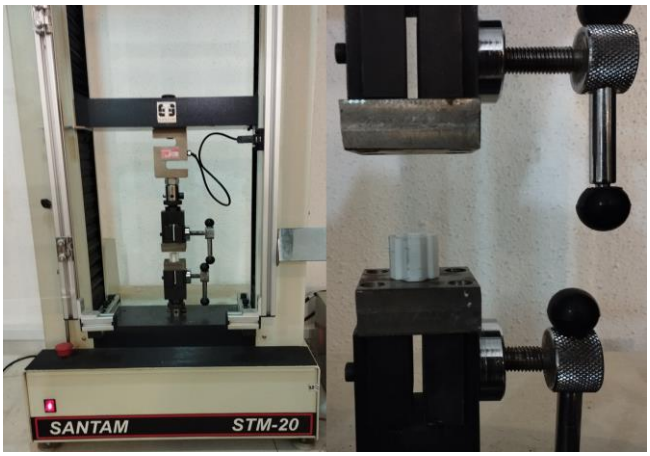

Fig. 4. SANTAM STM 20 Test Machine

Numerical modeling

The studied scutoid and honeycomb specimens are modeled in the SOLIDWORKS software, and the models are imported to the explicit dynamic module of the Abaqus software. As the models' walls are relatively thick compared to the dimensions of the specimens, the models are meshed with C3D10M solid elements. C3D10M is a 10-node modified quadratic tetrahedron which is well-suited for uniform mesh continuity and reduces computational time. To ensure the accuracy of element size, the mesh sensitivity analysis for the PCF parameter of the honeycomb specimen is conducted. Figure 5 shows the calculated PCF for the honeycomb specimen in relation to the element size. After performing the mesh size sensitivity analysis based on the PCF parameter, the mesh size of 0.3 mm is chosen and applied to all specimens, and the models are discretized with a total of 456,000-490,000 elements. Figure 6 shows a specimen that is meshed using this element size.

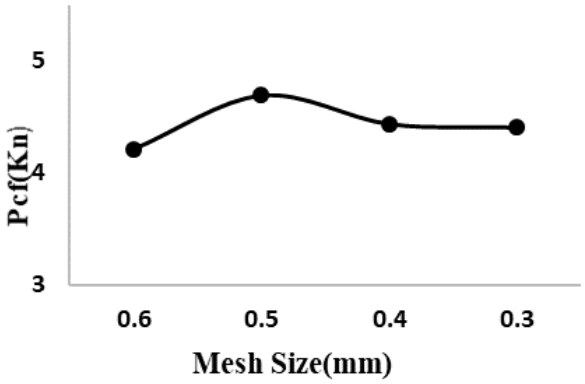

Fig. 5. Mesh sensitivity versus PCF

To model the quasi-static crushing test, two rigid plates are modeled at both ends of the specimens as the upper and lower platen of the compression test machine. The friction coefficient of 0.2 is defined in the contact surface between the rigid plates and the specimens [39,40]. The self-contact, i.e., the contact between the faces of the specimens itself, is also defined. The bottom rigid plate is assumed to be fixed and the upper rigid plate moves downward with constant speed.

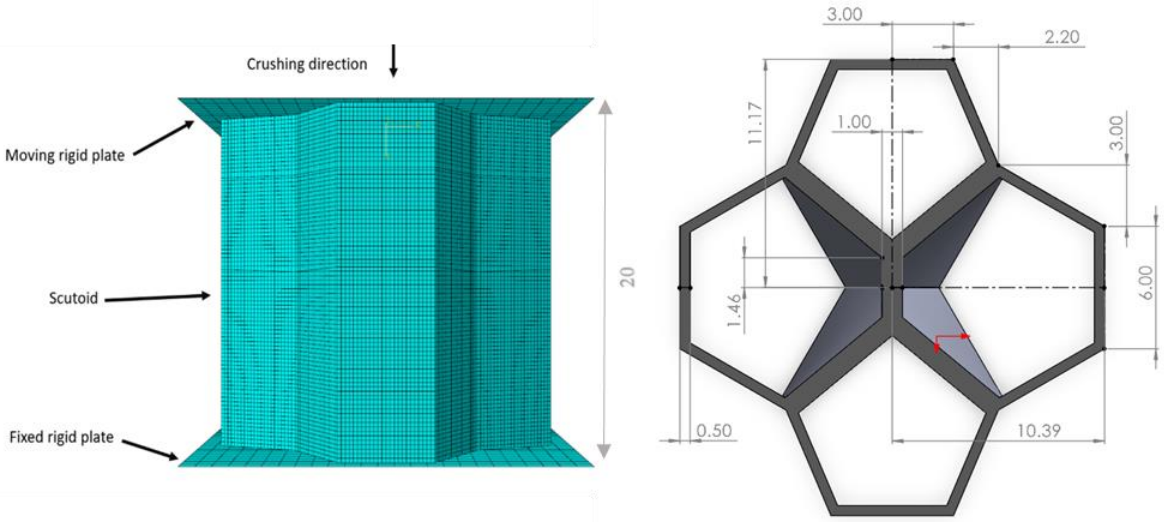

Fig. 6. Sample specifications of T50 (mm)

Moreover, to evaluate the accuracy of the quasi-static analysis in explicit dynamics, one should ensure that the total kinetic energy is small compared to the total internal energy and the ratio of kinetic energy to internal energy must be less than 5 % [41,42]. In Fig. 7, the kinetic energy to internal energy ratio is presented for the finite element crushing modeling of the honeycomb specimen, in which, the amount of kinetic energy is almost zero.

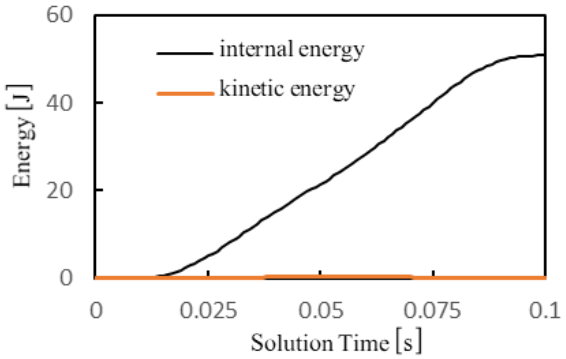

Fig. 7. A typical kinetic energy and internal energy versus solution time diagram

Results and Discussion

Numerical and experimental quasi-static compressive results

In this research, the crushing behavior and energy absorption of the 4-cell scutoids and honeycomb structures have been investigated in the quasi-static compression test. The crushing force-displacement curves for the honeycomb and scutoid specimens are extracted from the experiment and the numerical models. The numerical results for all specimens are illustrated in Fig. 8. The comparison of the force-displacement experimental and numerical diagrams is presented in Table 3. In which the bold line is the experimental result and the dashed line is the numerical result. The results indicate that the transition point location changes the compressive behavior and energy

absorption capability of the scutoids. The maximum crushing force for these specimens varies between 3.84 and 4.10 kN. The absorbed energy is between 34.69 and 39.67 and the crushing efficiency is between It varies from 62.84 to 71.28 %. The deformation of the specimens in different stages is, also, shown in Table 3.

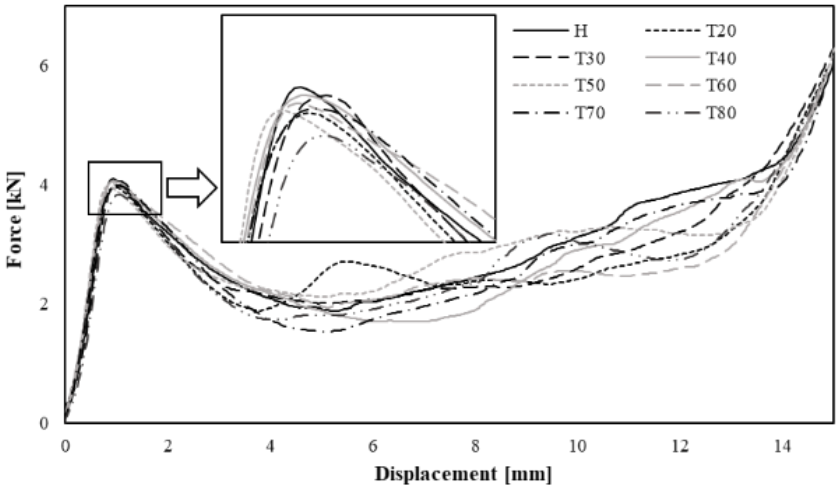

Fig. 8. The force-displacement curves from experiments for the honeycomb and scutoid specimens

Table 3. The comparison between the experimental and numerical results for the honeycomb specimen

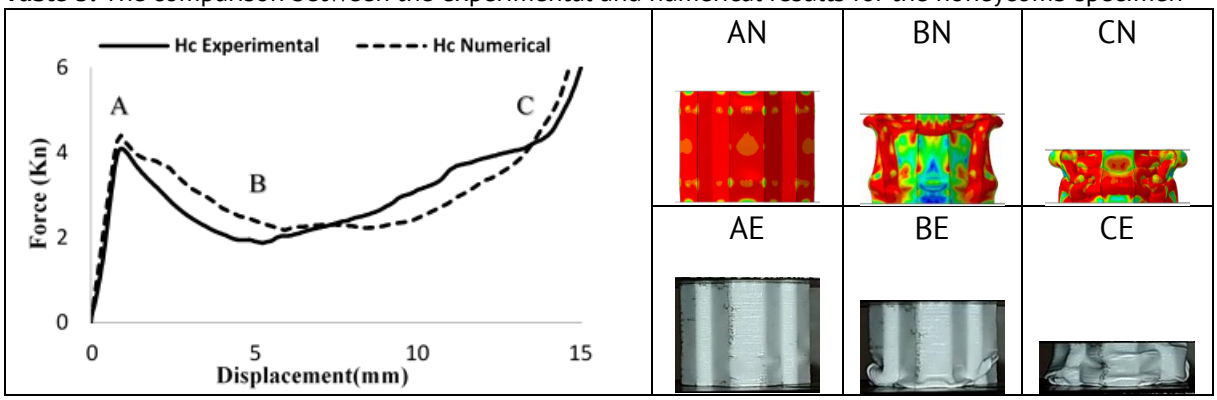

Under axial load, thin-walled cylindrical tubes usually fail in progressive folding buckling mode. While the failure modes for the square tubes are different. For the square tubes, the buckling shape develops when the load reaches the buckling load. By increasing the compressive load, the amplitude of the deformation increases, and many folds form simultaneously. Whereas, in progressive folding mode, each fold develops after the previous fold completion [43]. Chen [43] showed that the deformation modes of the uniform hexagonal honeycomb are similar to the symmetric deformation of the cylindrical tube.

The experimental and numerical results for the honeycomb and scutoid specimens are compared in Tables 3 and 4, respectively. The behavior of the studied honeycomb, in the numerical study, was like that of the cylindrical tubes. The buckling started by forming two folds on the honeycomb outer skin which is the thinnest part of the specimen. As the load increased, the folds grew larger. In contrast, in the experiment, due to the manufacturing imperfection at the ends, a fold started to form at the bottom first, and

another fold started to form after the first fold completion. The fluctuation in the experimental force-displacement curve is due to this phenomenon. From Table 4, it can be deduced that for all specimens, the buckling of all outer shells starts in the same manner. The outer shell first buckled in the upper and lower regions. Like the square tubes studied by Chen [43], the buckling shape amplitudes grew simultaneously.

Table 4. The comparison between the experimental and numerical results for the scutoid specimens (continued)

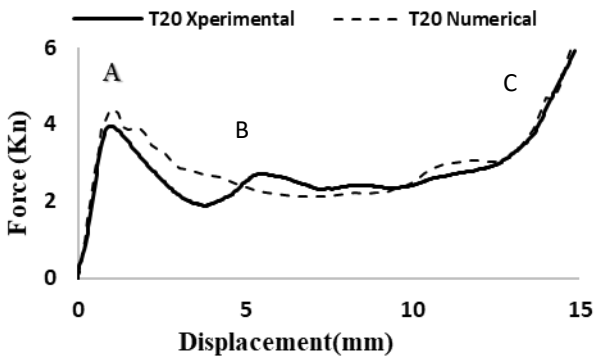	AN	BN	CN
	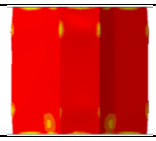	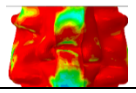	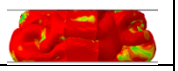
	AE	BE	CE
			
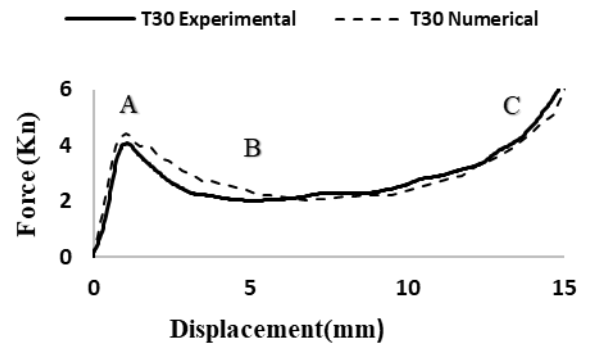	AN	BN	CN
	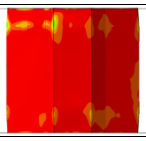	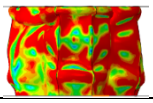	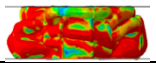
	AE	BE	CE
		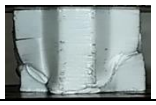	
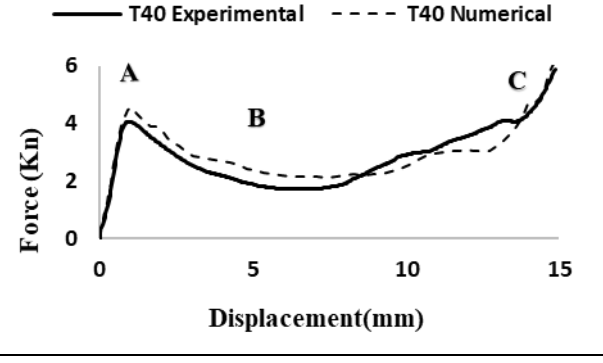	AN	BN	CN
	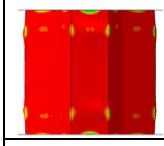	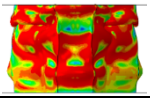	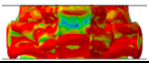
	AE	BE	CE
			
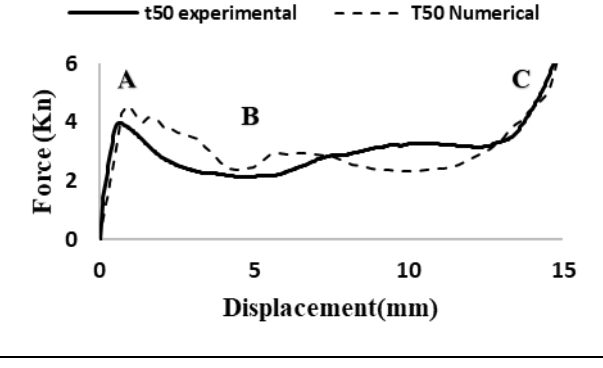	AN	BN	CN
	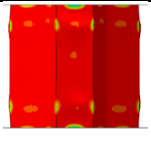	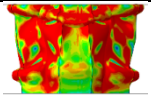	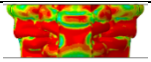
	AE	BE	CE
			

Table 4. The comparison between the experimental and numerical results for the scutoid specimens (continued)

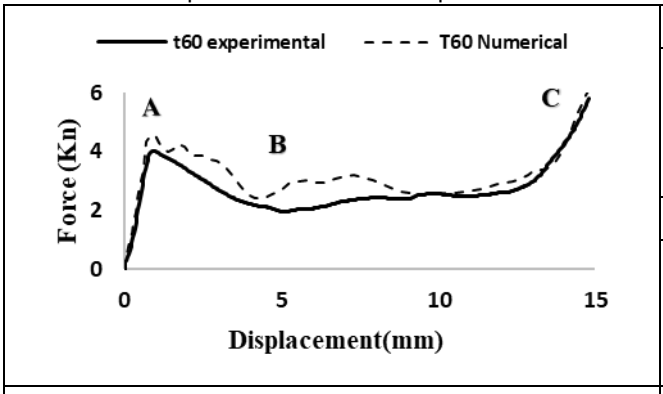	AN	BN	CN
	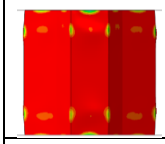	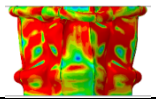	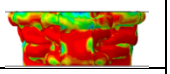
	AE	BE	CE
	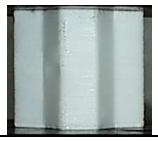		
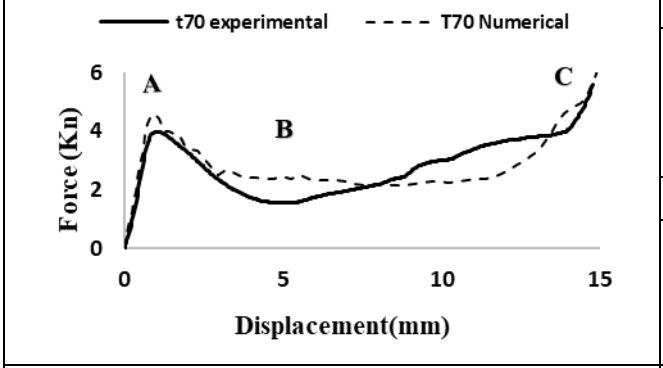	AN	BN	CN
	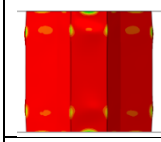	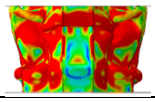	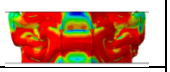
	AE	BE	CE
			
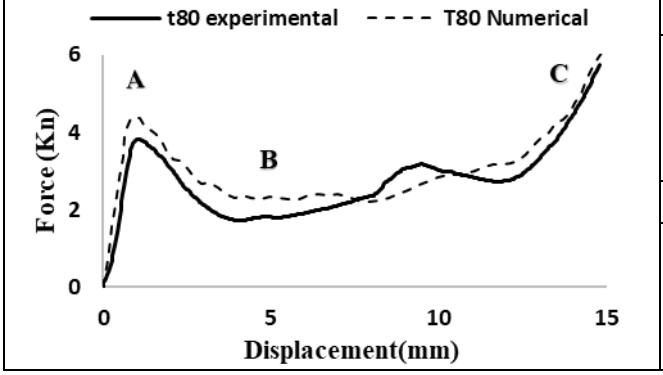	AN	BN	CN
	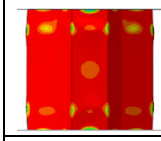	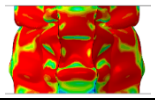	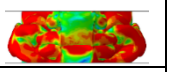
	AE	BE	CE
			

Energy absorption capacity assessment

The impact efficiency of the energy absorbers can be determined using various indices. Each of these indicators evaluates the behavior of the energy-absorbing structure by considering different aspects, i.e., Peak Crushing Force (PCF), Absorbed Energy (EA), Mean Crushing Force (MCF), Specific Absorbed Energy (SEA), and Crushing Efficiency (CLE) [44,45] as follows:

$$EA = \int_0^d F(x)dx \quad (1)$$

$$SEA = \frac{EA}{m} \quad (2)$$

$$MCF = \frac{EA}{d} \quad (3)$$

$$CLE = \frac{MCF}{PCF} \quad (4)$$

where $F(x)$, m and d are the collapse force at displacement x, the energy absorber mass and crushing length, respectively. Crushing length is the amount of force displacement in the crush test before densification. All indicators in the quasi-static collapse test are calculated until the beginning of the densification zone.

In this study, all specimens have the same mass, therefore, only PCF, EA, MCF and CLE are considered. For all samples, the amount of crushing length is the same and the effect of transition point can be determined better. Based on the force-displacement curves extracted from the numerical analysis, the energy absorption indices are calculated for T20 to T80, and the honeycomb specimens are shown in Table 5. Among these specimens, the amount of absorbed energy for the T50 specimen is higher than all the specimens. On the other hand, the amount of PCF for T80 and T20 is lower than all the structures. The reason is the collapse initiation in the inner shells in the top and bottom region, which leads to the collapse of some parts of the object in an inclined direction. Since the amount of energy divided by the crushing length gives the MCF value, the MCF value for the T50 specimen is, also, the highest, and the value of the crushing efficiency for T50, which is obtained by dividing the MCF by the PCF, is the highest.

Table 5. Energy absorption indices of scutoid specimens (experimental tests)

	***EA*, J**	***PCF*, KN**	***MCF*, KN**	***CLE*, %**	***SEA*, J/g**
T20	35.74	3.96	2.55	64.47	23.57
T30	37.49	4.05	2.68	66.12	24.80
T40	37.77	4.06	2.71	66.45	25.02
T50	40.56	3.97	2.90	72.98	26.87
T60	36.45	4.01	2.59	64.93	24.13
T70	37.49	3.98	2.68	67.28	24.78
T80	36.34	3.84	2.60	67.20	23.98
Hc	39.88	4.10	2.85	69.48	26.93

Failure mode assessment

In progressive buckling, the peak force indicates the beginning of the buckling process, which can be controlled by placing mechanisms to control the buckling onset and reduce the PCF value. When the crushing process starts, the structure enters the plastic region, the crushing load decreases, and the structure starts to fold. When the folding of this part of the member is completed, the load starts to increase until the plastic process occurs in the next place. This process is repeated until all the energy is absorbed or until the member cannot absorb any more energy. This stage is characterized by a sudden increase in load and is called densification.

In Figs. 9 and 10, the failure modes of 4-cell scutoids specimens and a honeycomb specimen from numerical analysis are presented. It should be noted that due to the lower thickness of the outer walls (0.5 mm), the commencement of the buckling and the failure of all specimens are when the outer walls of the specimens are buckled. For all specimens, the outer wall, first, buckled in the upper and lower regions in a symmetrical manner (Table 4 Point A). All specimens underwent the densification phase, which is the end of the energy absorption phase.

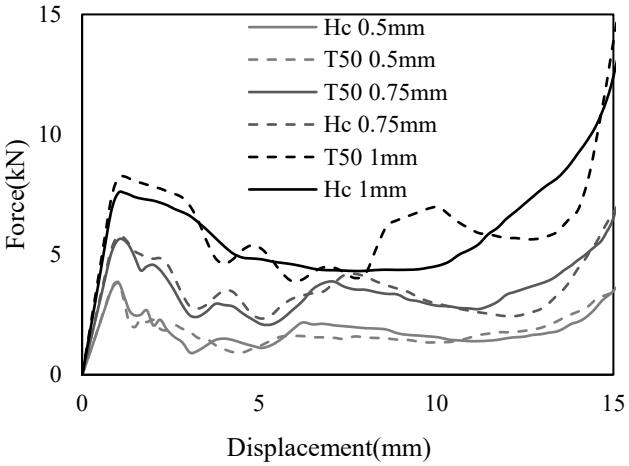

Fig.9. Force displacement diagram of T50 and Hc with diffrent thickness

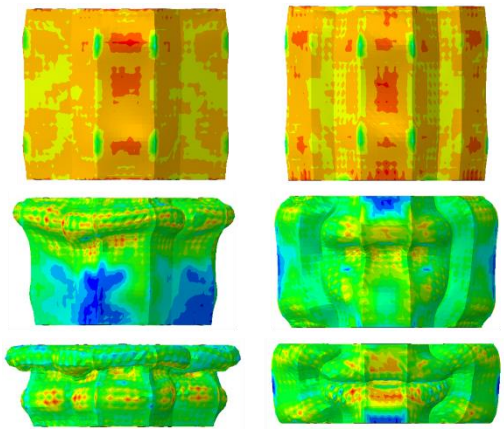

Fig. 10. Failure mode for T50 1mm and HC 1 mm from Group 2

Figure 11 compares the T50 and T20 specimens' deformation and the honeycomb specimen's deformation. T50 is the best specimen in energy absorption. The outer wall deformation of the three specimens is quite similar at the beginning. In the honeycomb specimen, after the outer shell buckling, increasing the displacement would cause the inner shells to buckle locally in the middle part. The inner shell buckling shape differed from the outer shell buckling shape. The outer shell buckled in a fold, whereas the inner shell buckled in 2 folds. In the T50 specimen, the outer shell buckling, also, affected the inner wall buckling, and the first two small buckling deformations on the outer wall shaped a two-fold deformation on the outer shells. The fold number of the inner shell of the T50 is 3 which is the biggest fold number of all specimens, and means that it deformed more effectively.

Scutoid specimens whose failure mode occurred away from the rigid plates have more energy absorption capacity, i.e., T40, T50, and T70 specimens. In addition to the energy absorption that was discussed, reducing the maximum crushing force is also required to increase the efficiency of the crushing load. In addition to these points, it has been pointed out that the type of external walls' failure mode has a great effect on the amount of energy absorption, for example, in specimens whose external walls are folded inwards during the crushing process, energy absorption is less, T20, T30, T60, and T80 specimens.

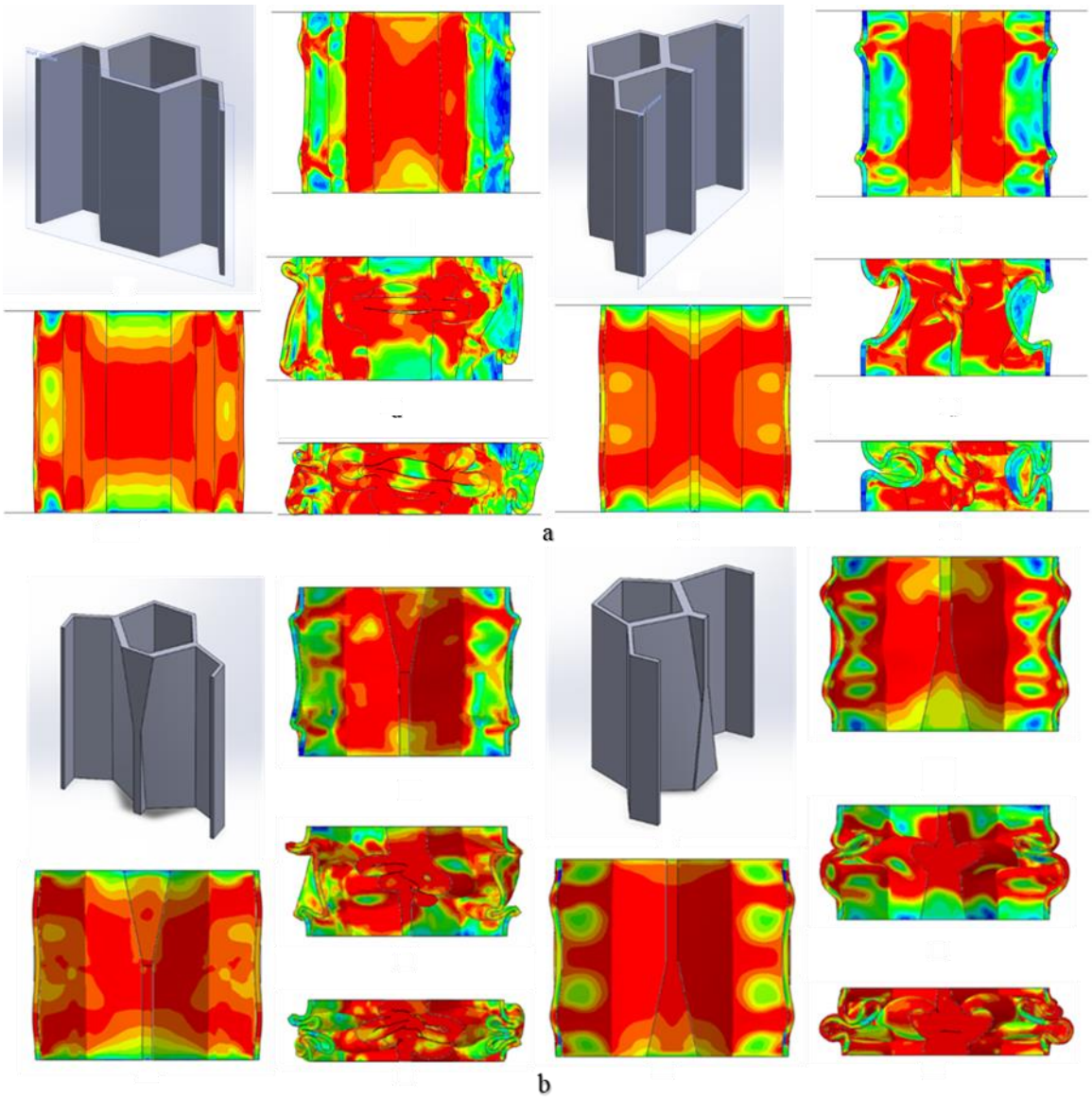

Fig. 11. A cut view of Hc specimen(a) and the T20 specimen (b)

The effect of thickness

In addition to the transition point location, the wall thickness also plays a significant role in the energy absorption characteristics of the scutoid and honeycomb structures. The force-displacement diagrams for the T50 0.5 mm, T50 0.75 mm, T50 1 mm, Hc 0.5 mm, Hc 0.75 mm, and Hc 1 mm specimens are presented in Fig. 9. T50 1 mm has higher PCF which makes it less efficient in energy absorption application compared to HC 1 mm, while better in the strength required applications. Although the deformation pattern for all specimens is alike in some aspects, the thicker specimens are more efficient in energy absorption due to more uniform loading pattern

Figure 10 shows a comparison of failure modes between a honeycomb structure (right) and a T50 scutoid structure (left), both with a wall thickness of 1 mm. The initial failure mode observed is local symmetric buckling at 5 mm of compression. The final failure mode is densification, which closely mirrors the modes observed in experimental specimens.

As shown in Table 6, increasing the wall thickness leads to higher values for all the evaluated energy absorption indices: EA, PCF, MCF, and CLE in both the T50 scutoid and the honeycomb specimens. This trend can be attributed to the increased resistance to deformation provided by thicker walls. Thicker walls require higher forces to initiate buckling and collapse, resulting in a higher PCF. Consequently, the structure absorbs more energy before failure, leading to an increase in EA. The MCF, which represents the average force sustained during the crushing process, also rises due to the enhanced resistance. This ultimately leads to an improvement in the CLE, indicating that thicker walls enable the structure to absorb energy more efficiently relative to the peak force. While the transition point location influences the deformation mode and fold formation, the wall thickness acts as a global factor affecting the overall strength and energy absorption capacity of both the scutoid and honeycomb structures.

Table 6. The effect of the thickness on scutoid energy absorption

	***EA*, J**	***PCF*, kN**	***MCF*, kN**	***CLE*, %**	***SEA*, J/g**
T50 0.5 mm	23.84	3.82	1.70	44.5	20.37
Hc 0.5 mm	24.581	3.78	1.75	46.4	21.31
T50 0.75 mm	46.44	5.59	3.31	59.3	28.3
Hc 0.75 mm	47.14	5.78	3.36	58.2	27.8
T50 1 mm	80.49	8.25	5.75	69.6	35.94
Hc 1 mm	78.31	7.60	5.60	73.5	36.48

Based on Fig. 12, at a wall thickness of 0.5 mm, the Specific Energy Absorption (SEA) of the honeycomb structure surpasses that of the T50 specimen. However, at a wall thickness of 0.75 mm, the T50 specimen exhibits a higher SEA than the honeycomb structure. This trend reverses again at a wall thickness of 1 mm, where the honeycomb structure demonstrates a greater SEA value compared to T50. While increasing the wall thickness generally leads to an increase in energy absorption for both specimen types, this enhancement does not consistently favor either the honeycomb or the T50 structure. The inconsistent very small superiority between the two structures with increasing thickness indicates that simply increasing thickness and mass does not guarantee a superior SEA performance for either configuration.

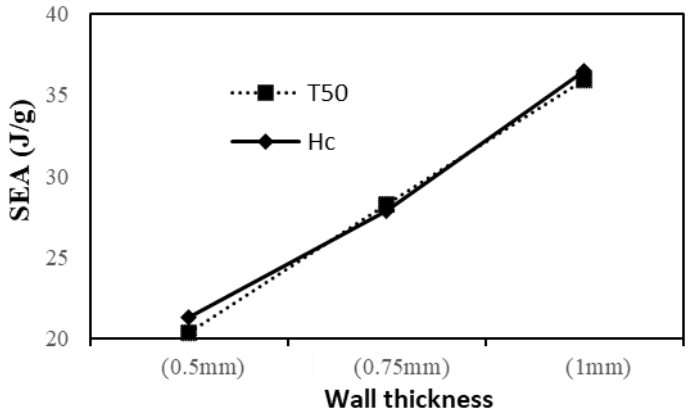

Fig. 12. The comparison of the SEA of T50 and HC from Group A

Figure 13 illustrates a comparative analysis of Specific Energy Absorption (SEA) values between our Group A (scutoids) and Group B (T50s and HCs) specimens and those reported by Cetin and Baykasoğlu for cubic lattice-filled specimens (LM 4 mm, 5 mm, and 6 mm). Notably, the HCS specimen exhibits the highest SEA among all samples. The scutoid from Group B specimens performs favourably relative to the specimens from Cetin and Baykasoğlu [12]. The scutoid and Hc specimens demonstrate competitive SEA values, generally outperforming the 4 mm and 5 mm LM specimens while exhibiting comparable performance to the 6 mm LM samples.

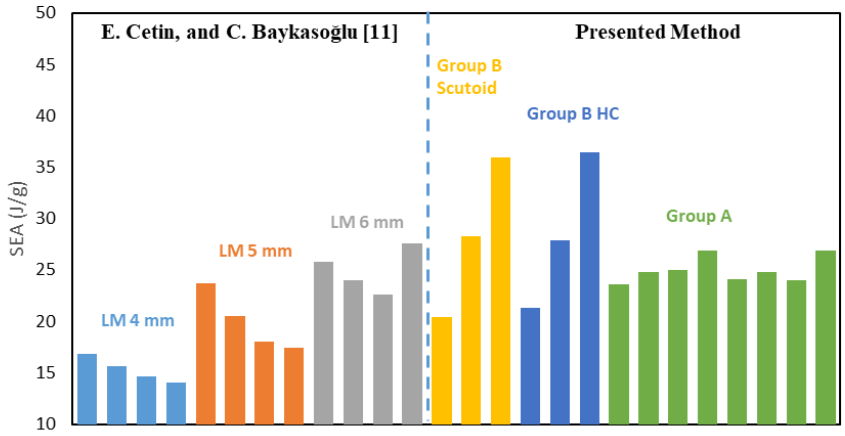

Fig. 13. Comparative analysis of Specific Energy Absorption (SEA) for scutoids & Hc, T50S, HCS, and cubic lattice-filled specimens (LM) with varying thicknesses. Based on [12]

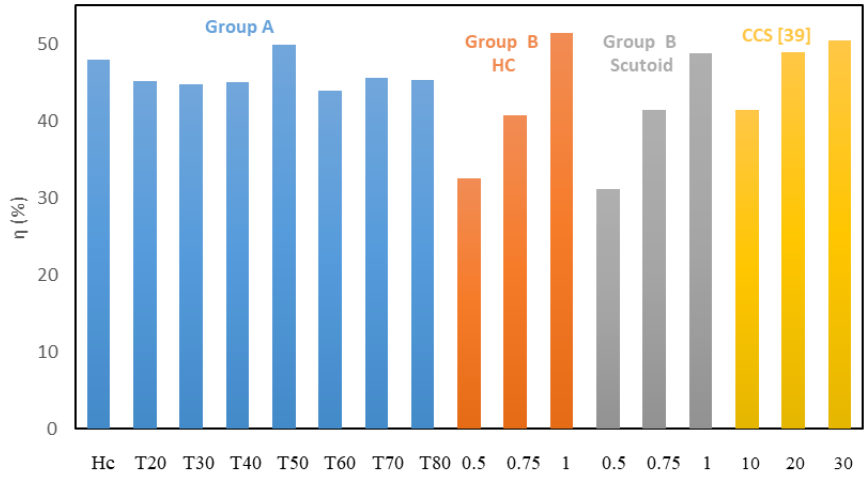

Fig. 14. Comparison of energy absorption efficiency (η) between scutoids, HC, T50, 3D cross–chiral auxetic materials. Based on [46]

Figure 14 presents a comparison of energy absorption efficiency(η), equivalent to CLE, between presented specimens and the 3D cross–chiral auxetic materials studied by Wang et al. [46] Scutoid specimens exhibit η values ranging from approximately 44 to 50 %, while HC specimen displays an η of around 48 %. The T50 specimens from Group B, with varying thicknesses, show a range of η from approximately 32 to 51 %. In comparison, the CCS specimens from Wang et al. [46] demonstrate η values between

roughly 41 and 50 %, indicating a comparable energy absorption efficiency to scutoid specimens.

DOE analysis

To systematically investigate the effects of key geometric parameters on crushing performance, a 2^3 full factorial Design of Experiments (DOE) was employed. The factors investigated were transition point height (h), inner wall thickness (t_{in}), and outer wall thickness (t_{out}), with crushing load efficiency (CLE) and specific energy absorption (SEA) as the primary response variables.

The DOE matrix consisted of eight simulation runs combining two levels of each factor (h = 20, 50 mm; t_{in} = 0.5, 1 mm; t_{out} = 0.5, 1 mm). The FEM simulations were performed according to this full factorial matrix, enabling systematic variation of parameters to capture their individual and interactive effects.

Analysis of Variance (ANOVA) was applied to the simulation results to identify statistically significant factors influencing CLE and SEA. The results confirm that inner wall thickness (t_{in}) is the most influential parameter for both responses. Increasing t_in improved both CLE and SEA due to the higher structural stiffness and delayed local buckling. Outer wall thickness (t_{out}) also played a meaningful role, particularly in SEA enhancement, while transition height (H) contributed less strongly but still showed a noticeable effect.

Updated ANOVA observations based on the 8-point dataset revealed the following relationships:

1. t_{in} ($p < 0.01$) and t_{out} ($p < 0.05$) significantly influenced CLE, accounting for 74 % of the total variance (R^2 = 0.74).
2. t_{in} ($p < 0.01$) and h ($p < 0.05$) dominated SEA variations, with a model fit of R^2 = 0.81.
3. A notable $h \times t_{out}$ interaction ($p < 0.1$) affected SEA, indicating non-linear sensitivity when both parameters increase simultaneously.

Table 7. The effect of the thickness on scutoid energy absorption

h, mm	t_{in}, mm	t_{out}, mm	CLE, %	SEA, J/g
20	0.5	0.5	49	21.38
20	1	0.5	64	23.51
20	0.5	1	62	28.29
20	1	1	73	34.34
50	0.5	0.5	45	20.38
50	1	0.5	70	35.94
50	0.5	1	68	31.84
50	1	1	70	78.31

The DOE matrix (Table 7) demonstrated:

1. The highest SEA occurred at t_{in} = 1 mm, t_{out} = 1 mm, h = 50 mm, with a value of 78.31 J/g.
2. The maximum CLE was also observed at t_{in} = 1 mm, t_{out} = 1 mm, h = 20 mm, yielding 73 %, though a similarly high value of 70 % appeared at h = 50 mm.

These results show that increasing both wall thicknesses enhances energy absorption, while transition height has a mixed influence—raising h improves SEA

substantially in thick-wall configurations but reduces CLE in thin-wall cases, highlighting a performance trade-off.

This DOE approach enabled efficient exploration of the geometric design space using a limited number of FEM simulations. The findings confirm the critical role of inner wall thickness in maximizing both crushing efficiency and energy absorption, while interactions with outer thickness and transition height must be considered for multi-objective optimization of crushing components.

Conclusions

In this research, the crushing behavior and crashworthiness of the scutoid structure have been investigated using numerical and experimental methods. Seven 4-cell self-packing scutoids and a 4-cell equivalent honeycomb were designed, fabricated using PLA filament through additive manufacturing, and tested under quasi-static compression. Numerical models were developed in Abaqus to simulate the crushing behavior, and the results were compared with experimental data, showing good agreement.

Seven four-cell self-packing scutoids and a four-cell equivalent honeycomb structure were designed and analyzed. The key findings of this study are:

1. Scutoid structures exhibited superior energy absorption capabilities compared to traditional honeycomb structures.
2. The energy absorption of scutoids was directly related to the number of folds formed during crushing. More folds resulted in higher energy absorption.
3. The location of the transition point in a scutoid significantly influenced its energy absorption efficiency. Scutoids with a transition point near the middle of their height demonstrated the highest energy absorption efficiency.
4. The honeycomb specimen exhibited a nearly symmetrical buckling shape in both the outer and inner shells.

Furthermore, the investigation into the effect of wall thickness on the T50 scutoid and honeycomb specimens revealed that increasing the wall thickness resulted in higher values for all the evaluated energy absorption indices (EA, PCF, MCF, and CLE). This finding highlights the significant role of wall thickness as a global factor influencing the overall strength and energy absorption capabilities of both the scutoid and honeycomb structures.

In conclusion, both the location of the transition point and the wall thickness are crucial design parameters that significantly impact the energy absorption performance of scutoid structures. By optimizing these parameters, it is possible to enhance the crashworthiness and energy absorption capabilities of these bio-inspired cellular structures for various applications.

CRediT authorship contribution statement

Sepahvand Yasin: writing – original draft, software, validation, formal analysis, investigation, data curation, writing – original draft; **Morshedsolouk Fattaneh:** methodology, data curation, supervision, writing – review & editing; **Moazemi Goudarzi Ali:** conceptualization, methodology, data curation, supervision.

Conflict of interest

The authors declare that they have no conflict of interest.

References

1. Bhutada S, Goel M. Crashworthiness parameters and their improvement using tubes as an energy absorbing structure: an overview. *International Journal of Crashworthiness*. 2022;27(6): 1569–1600.
2. Abdullah NAZ, Sani MSM, Salwani MS, Husain NA. A review on crashworthiness studies of crash box structure. *Thin-Walled Structures*. 2020;153: 106795.
3. Alexander JM. An approximate analysis of the collapse of thin cylindrical shells under axial loading. *The Quarterly Journal of Mechanics and Applied Mathematics*. 1960;13(1): 10–15.
4. Abramowicz W, Jones N. Dynamic axial crushing of circular tubes. *International Journal of Impact Engineering*. 1984;2(3): 263–281.
5. Abramowicz W, Jones N. Dynamic axial crushing of square tubes. *International Journal of Impact Engineering*. 1984;2(2): 179–208.
6. Tak SK, Iqbal MA. Axial compression behavior of thin-walled mild steel tubes subjected to axial impact. *Materials Physics and Mechanics*. 2021;47(5): 681–696.
7. Yamada Y, Banno T, Xie Z, Wen C. Energy absorption and crushing behaviour of foam-filled aluminium tubes. *Materials Transactions*. 2005;46(12): 2633–2636.
8. Zarei H, Kröger M. Optimization of the foam-filled aluminum tubes for crush box application. *Thin-Walled Structures*. 2008;46(2): 214–221.
9. Li Z, Yu J, Guo L. Deformation and energy absorption of aluminum foam-filled tubes subjected to oblique loading. *International Journal of Mechanical Sciences*. 2012;54(1): 48–56.
10. Najibi A, Ghazifard P, Alizadeh P. Numerical crashworthiness analysis of a novel functionally graded foam-filled tube. *Journal of Sandwich Structures and Materials*. 2021;23(5): 1635–1661.
11. Baykasoğlu A, Baykasoğlu C, Cetin E. Multi-objective crashworthiness optimization of lattice structure filled thin-walled tubes. *Thin-Walled Structures*. 2020;149: 106630.
12. Cetin E, Baykasoğlu C. Crashworthiness of graded lattice structure filled thin-walled tubes under multiple impact loadings. *Thin-Walled Structures*. 2020;154: 106849.
13. Tao C, Zhou X, Liu Z, Liang X, Zhou W, Li H. Crashworthiness study of 3D printed lattice reinforced thin-walled tube hybrid structures. *Materials*. 2023;16(5): 1871.
14. Le D, Novak N, Arjunan A, Baroutaji A, Estrada Q, Tran T, Le H. Crashworthiness of bio-inspired multi-stage nested multi-cell structures with foam core. *Thin-Walled Structures*. 2023;182: 110245.
15. Nikkhah H, Baroutaji A, Kazancı Z, Arjunan A. Evaluation of crushing and energy absorption characteristics of bio-inspired nested structures. *Thin-Walled Structures*. 2020;148: 106615.
16. Hosseinpour E, Goudarzi AM, Morshedsolouk F, Gharehbaghi H. Numerical and experimental study on the energy absorption characteristics of thin-walled auxetic cylindrical tubes with varying porosity. *Journal of Materials Research and Technology*. 2025;39: 400-417.
17. Nikkhah H, Baroutaji A, Olabi AG. Crashworthiness design and optimisation of windowed tubes under axial impact loading. *Thin-Walled Structures*. 2019;142: 132–148.
18. Rogala M, Gajewski J. Crashworthiness analysis of thin-walled square columns with a hole trigger. *Materials*. 2023;16(11): 4196.
19. Tran T, Baroutaji A, Estrada Q, Arjunan A, Le H, Thien N. Crashworthiness analysis and optimization of standard and windowed multi-cell hexagonal tubes. *Structural and Multidisciplinary Optimization*. 2021;63: 2191–2209.
20. Taghipoor H, Ghiaskar A, Shavalipour A. Crashworthiness performance of thin-walled square tubes with circular hole discontinuities under high-speed impact loading. *International Journal of Crashworthiness*. 2022;27(6): 1622–1634.
21. El-baky MAA, Allah MMA, Kamel M, Abd-Elaziem W. Energy absorption characteristics of E-glass/epoxy over-wrapped aluminum pipes with induced holes: experimental research. *Scientific Reports*. 2022;12(1): 21097.
22. Borovkov A, Maslov L, Zhmaylo M, Tarasenko F, Nezhinskaya L. Elastic properties of additively produced metamaterials based on lattice structures. *Materials Physics and Mechanics*. 2023;51(7): 42–62.

23. Baroutaji A, Arjunan A, Stanford M, Robinson J, Olabi AG. Deformation and energy absorption of additively manufactured functionally graded thickness thin-walled circular tubes under lateral crushing. *Engineering Structures*. 2021;226: 111324.
24. Nian Y, Wan S, Zhou P, Wang X, Santiago R, Li M. Energy absorption characteristics of functionally graded polymer-based lattice structures filled aluminum tubes under transverse impact loading. *Materials & Design*. 2021;209: 110011.
25. Nian Y, Wan S, Li X, Su Q, Li M. How does bio-inspired graded honeycomb filler affect energy absorption characteristics? *Thin-Walled Structures*. 2019;144: 106269.
26. Gharehbaghi H, Farrokhabadi A. Parametric study of the energy absorption capacity of 3D-printed continuous glass fiber reinforced polymer cruciform honeycomb structure. *Steel and Composite Structures*. 2022; 49(4): 393–405.
27. Gharehbaghi H, Farrokhabadi A, Noroozi Z. Introducing a new hybrid surface strut-based lattice structure with enhanced energy absorption capacity. *Mechanics of Advanced Materials and Structures*. 2024;31(14): 2955–2964.
28. Ghorbani F, Gharehbaghi H, Farrokhabadi A, Bolouri A. Evaluation of the mechanical properties and energy absorption in a novel hybrid cellular structure. *Aerospace Science and Technology*. 2024;148: 109105.
29. Ghorbani F, Gharehbaghi H, Farrokhabadi A, Bolouri A. Investigation of the equivalent mechanical properties of the bone-inspired composite cellular structure: analytical, numerical and experimental approaches. *Composite Structures*. 2023;309: 116720.
30. Galehdari SA, Kadkhodayan M, Hadidi-Moud S. Low velocity impact and quasi-static in-plane loading on a graded honeycomb structure: experimental, analytical and numerical study. *Aerospace Science and Technology*. 2015;47: 425–433.
31. Guo Y, Chen L, Zhu C, Liu H, Pan X, Du B, Zhao W, Li W. Fabrication and axial compression test of thermoplastic composite cylindrical sandwich structures with hierarchical honeycomb core. *Composite Structures*. 2021;275: 114453.
32. Usta F, Scarpa F, Türkmen HS. Edgewise compression of novel hexagonal hierarchical and asymmetric unit cells honeycombs metamaterials. *Materials Today Communications*. 2020;24: 101102.
33. Feng G, Li S, Xiao L, Song W. Energy absorption performance of honeycombs with curved cell walls under quasi-static compression. *International Journal of Mechanical Sciences*. 2021;210: 106746.
34. Xia P, Liu Q, Fu H, Yu Y, Wang L, Wang Q, Yu X, Zhao F. Mechanical properties and energy absorption of 3D printed double-layered helix honeycomb under in-plane compression. *Composite Structures*. 2023;315: 116982.
35. Nikkhah H, Crupi V, Baroutaji A. Crashworthiness analysis of bio-inspired thin-walled tubes based on Morpho wings microstructures. *Mechanics Based Design of Structures and Machines*. 2022;50(10): 3683–3700.
36. Tao Y, Li W, Wei K, Duan S, Wen W, Chen L, Pei Y, Fang D. Mechanical properties and energy absorption of 3D printed square hierarchical honeycombs under in-plane axial compression. *Composites Part B: Engineering*. 2019;176: 107219.
37. Gómez-Gálvez P, Vicente-Munuera P, Tagua A, Forja C, Castro AM, Letrán M, Valencia-Expósito A, Grima C, Bermúdez-Gallardo M, Serrano-Pérez-Higueras Ó. Scutoids are a geometrical solution to three-dimensional packing of epithelia. *Nature Communications*. 2018;9(1): 2960.
38. Dhari RS, Patel NP. On the crushing behaviour of scutoid-based bioinspired cellular structures. *International Journal of Crashworthiness*. 2022;27(4): 945–954.
39. Hu L, Luo Z, Yin Q. Negative Poisson's ratio effect of re-entrant anti-trichiral honeycombs under large deformation. *Thin-Walled Structures*. 2019;141: 283–292.
40. Wei L, Zhao X, Yu Q, Zhang W, Zhu G. In-plane compression behaviors of the auxetic star honeycomb: experimental and numerical simulation. *Aerospace Science and Technology*. 2021;115: 106797.
41. Chen J, Fang H, Liu W, Zhu L, Zhuang Y, Wang J, Han J. Energy absorption of foam-filled multi-cell composite panels under quasi-static compression. *Composites Part B: Engineering*. 2018;153: 295–305.
42. Tasdemirci A, Sahin S, Kara A, Turan K. Crushing and energy absorption characteristics of combined geometry shells at quasi-static and dynamic strain rates: experimental and numerical study. *Thin-Walled Structures*. 2015;86: 83–93.
43. Chen D-h. Crush mechanics of thin-walled tubes. Book. CRC Press; 2018.
44. Jones N. Energy-absorbing effectiveness factor. *International Journal of Impact Engineering*. 2010;37(6): 754–765.
45. Kotełko M, Ferdynus M, Jankowski J. Energy absorbing effectiveness–different approaches. *Acta Mechanica et Automatica*. 2018;12(1): 54–59.
46. Wang Q, Yang Z, Lu Z, Li X. Mechanical responses of 3D cross-chiral auxetic materials under uniaxial compression. *Materials & Design*. 2020; 186:108226.